Acta Crystallographica Section D
Biological Crystallography
ISSN 0907-4449

Surface morphology and kinetic properties in rapid growth of EAFP protein crystals investigated by atomic force microscopy

Sheng Wang,[a,b] Genpei Li,[a,b] Ye Xiang,[a] Ren-Huai Huang,[a] Ying Zhang[a] and Da-Cheng Wang[a,b]*

[a]Center for Structural and Molecular Biology, Institute of Biophysics, Chinese Academy of Sciences, Beijing 100101, People's Republic of China, and [b]National Microgravity Laboratory, Chinese Academy of Sciences, Beijing 100080, People's Republic of China

Correspondence e-mail: dcwang@sun5.ibp.ac.cn

Received 21 July 2004
Accepted 28 April 2005

The whole process of EAFP protein monoclinic crystal growth with an extremely fast rate has been observed by atomic force microscopy. The results showed that the patterns of the growth images in rapidly growing crystals are complicated. The two-dimensional multi-layered stacks of growth steps are characteristic of higher supersaturation and the growth of steps proceeds in a manner of strong anisotropic spiral dislocations dominantly under lower supersaturation conditions. The complex dislocation sources, including multiple dislocation and multi-interacting single dislocation sources, the constant step-split and the propagation of trooped steps were observed on the {100} surfaces of growing EAFP crystals. The step height of each layer generated either by two-dimensional nucleation at higher supersaturation or by screw dislocation at lower supersaturation is about 2–3 nm, which corresponds to the length of the crystallographic unit cell. Although the rate of advancement for each growth step is similar to that of other protein crystal growth, the unique way of the propagation distinct with the trooped steps, by which a bundle of steps are strapped together, would be responsible for the rapid growth of EAFP crystals. All features show a possible mechanism by which the fast growth of EAFP crystals could be attained. The structural basis of the growth mechanism is also discussed.

1. Introduction

In the practice of protein crystallization, we know that some proteins require a rather long time, such as several months, to be crystallized with good quality, but others need only short times of a day or hours. To date, the crystal growth of a number of proteins has been investigated by atomic force microscopy (AFM; *e.g.* Astier *et al.*, 2001; Durbin & Carlson, 1992; Kuznetsov *et al.*, 1996; Land & De Yoreo, 2000; Malkin *et al.*, 1999; McPherson *et al.*, 2001; Yip & Ward, 1996). Some mechanisms of protein crystal growth with normal rates have been revealed (Land *et al.*, 1995; Kuznetsov *et al.*, 1995, 1996; Malkin *et al.*, 1995). However, the growth behaviours of those protein crystals that grow with very fast rates are largely unknown to date. Here, we report the crystal-growth process of the *Eucommia* antifungal protein (EAFP) growing with an extremely fast rate by *in situ* AFM observation, which revealed certain kinetic properties for the fast growth of protein crystal.

EAFP is purified from the bark of the tree *Eucommia ulmoides* Oliv and consists of 41 amino-acid residues; it is a novel type of antifungal protein with a distinct five-disulfide cross-linked scaffold (Liu *et al.*, 1994; Huang *et al.*, 2002). EAFP can be crystallized as a monoclinic form within several hours over wide pH range (4.5–7.8; Xiang *et al.*, 2002). The crystals diffract to atomic resolution (~0.8 Å) and exhibit minimum decay on exposure to X-ray radiation. The preliminary crystallographic analysis and structural solution have been carried out recently (Xiang *et al.*, 2004). These provide a valuable chance to investigate the mechanism of rapid growth of a protein crystal. In this paper the surface morphology, growth kinetics and intermolecular interactions in the fast growth process will be described and the possible mechanism distinct for rapid growth will be discussed.

2. Experimental

2.1. Materials and methods

The protein sample used in crystallization was isolated from the bark of the tree *E. ulmoides* Oliv and highly purified by several chromatography steps. The details of the procedure have been described previously (Huang *et al.*, 2002). All chemicals used in the present work were of analytical grade and all solutions were filtered with a microfilter of 0.22 µm diameter.

The monoclinic form crystals of EAFP were grown by the hanging-drop vapor-diffusion method in a solution containing 20 mg ml^{-1} EAFP buffered at pH 5.5 with 1.5 *M* NaAc and 1 *M* HAc in an incubator at 293 K. Under these conditions, the crystals were easily grown up to 0.8 × 0.2 × 0.06 mm in size and had a plate-like shape. Interestingly, the crystals were quickly visible (20–30 µm in size) when the crystallizing drop was disturbed by a needle tip after set up for 1 h. The crystals used in AFM observation were grown on a cover glass slide. The target crystals adhered tightly to the glass slide even after removal of the growth solution. The cover slide with the crystals was then transferred to the AFM sample stage for acquisition of AFM images (see Fig. 1).

2.2. AFM examination

The acquisition of AFM images was performed in both tapping and contact mode at the {100} faces of the EAFP monoclinic crystals with fluid cell. All observations were carried out using AutoProbe Thermomicroscopes (Park Scientific Inst.ruments, Sunnyvale, CA, USA) under the crystallization conditions. During the image acquisition, a weak force constant of ∼0.03 N m^{-1} was used throughout. The driving frequency was between 8 and 10 kHz. The set point was kept 5–10% below the free cantilever amplitude. Scan rates varied between 0.5 and 2 Hz according to scan sizes. In order to minimize the force applied to the surface when operating in contact mode, care was taken to continually adjust the set-point voltage to the lowest possible value. The only image processing was contrast adjustment. Mostly, no image smoothing or noise removal was carried out unless there were exceptional needs in special cases.

The relevant concentrations of the EAFP protein were determined with the standard calibrated curve with the interpolation method and the calibrated curve made from the UV absorbance at a wavelength of 280 nm. Supersaturation is defined as $\sigma = \ln(C/C_e)$, where C is the actual protein concentration of the solution and C_e is the equilibrium concentration at the crystallization temperature of the experiment.

The correlation of the crystal external shape with its crystallographic system (face indexing) and the unit-cell parameters were determined from X-ray diffraction patterns by using the Quantum-four-dimensional CCD area detector at beamline BL-18B station in Photon Factory, Tsukuba, Japan. The molecular interactions in the crystal were calculated with *CCP*4 suite of programs (Collaborative Computational Project, Number 4, 1994) and inspected with *O* (Jones *et al.*, 1991).

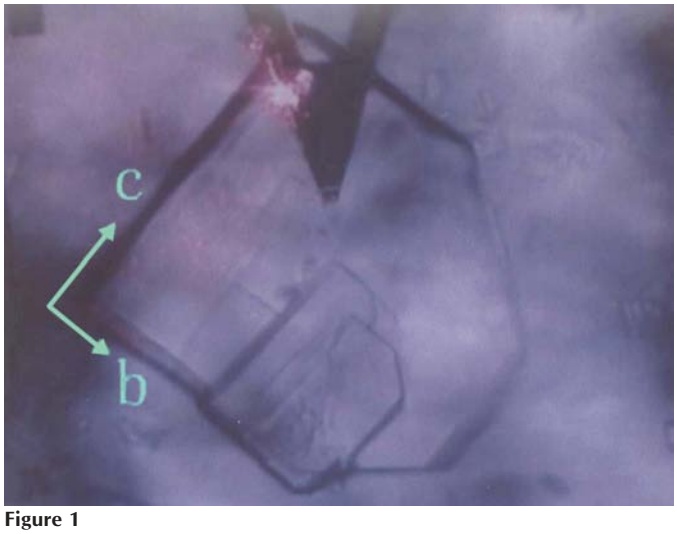

Figure 1
The setup of the AFM experiment. The EAFP crystal and cantilever tip above it are shown in the photograph. The correlation between external shape and crystallographic axis of the crystal is indicated by arrows. A colour version of this figure is available in the online edition of the journal.

3. Results and discussion

3.1. Kinetics and mechanism

3.1.1. Growth source. The growth sources and their development are complicated and they strongly depend upon growth conditions. As seen in Figs. 2(*a*)–2(*d*), at higher supersaturations (σ = ∼1.5), the dominant growth sources of growth steps were complex and active multiple-stacked two-dimensional nucleation, which exhibit strong anisotropy, and their number in the unit area of the growing surface was estimated to be about 5.7 × 10^6 cm^{-2} by means of counting the actual number of growth sources observed in various known scan areas according to the suggestion of Malkin *et al.* (1996). No screw dislocation sources virtually were found on any EAFP crystallizations examined at higher supersaturation; however, on the other hand, the strong asymmetric screw dislocation sources in various pictures, as shown in Figs. 3(*a*)–3(*d*), exhibit predominant growth sources at relatively lower supersaturations (σ = ∼0.8) and all these occurrences and the evolution of the active growth sources in EAFP crystals are generally similar to those of most other protein crystallizations investigated so far (Kuznetsov *et al.*, 1996). The growth spiral also contains a hollow core at the hillock, as described recently by McPherson and Land in their AFM studies (McPherson *et al.*, 1996, 2001; Land & De Yoreo, 2000). However, the apparent patterns of dislocation sources on the surfaces of growing crystals showed quite complex pictures and the number of the sources on the unit area of the surface was estimated to be ∼2.7 × 10^6 cm^{-2}, which was about six times more than that of other protein crystallizations. They contain main interacting double left-handed spirals (some coexisting weak right-handed dislocations also appeared at the vicinity of the main source core), which show a quite asymmetric shape and denseness of steps relative to the ⟨011⟩ or distortion typically along the ⟨011⟩ direction (Fig. 3). Apparently, the number of the growth sources and their multiplicity observed here in EAFP crystallization are somewhat different to those observed in other protein crystallizations.

3.1.2. Growth steps. The advancement and motion of individual steps on the {100} face of the EAFP crystal also strongly depends upon growth conditions. As seen in Fig. 2, at the higher supersaturation, the two-dimensional nuclei form a stack and expand in both the normal direction and the epitaxic mesa process. The growth of steps on the {100} face proceeded by spreading and merging of the troop or multiple-monomolecular layers and multilayers by multilayer step anisotropic advancement. The two- and three-dimensional nucleations form stacks over of 10–20 monolayers followed by layer-by-layer advancement of the ∼2 nm monomolecular steps. The rate of each step advancement in the [010] direction was estimated to be ∼4.5 × 10^{-6} cm s^{-1}, which is comparable with that from lysozyme crystal growth (Durbin & Carlson, 1992), but almost ten times faster than that measured from the thaumatin crystal (Kuznetsov *et al.*,

1996). The rate of two-dimensional expansion was found to be around six unit cells per second at the higher supersaturation. It is noticed that the growth rates of each growing step for EAFP crystals were the same order in magnitude as those of other protein crystals. Therefore, this continued advancement of the grouped steps might be responsible for the rapid growth of the EAFP crystal.

The advancement of the growth steps is quite different in varying directions. The rate of the advancement along the [001] direction is about four times faster than that along the [010] direction. The shape of the two-dimensional island is similar to that of its microcrystal or small crystal. Interestingly, at the lower supersaturation, the evolution of the growth steps for EAFP crystal showed some features distinct from other protein crystals. The nascent single steps and the macro-step in this condition exhibited a largely elongated shape in spiral growth. The growth steps appeared in troop and their advancement is also observed in sequential images *in situ* AFM examination. (Figs. 3*e* and 3*f*). In addition, the steps near the main left dislocation source are constantly split to give rise to certain right-handed spirals (Figs. 3*a*–3*d*), which form the additional growing source during development of the crystal surface. This step-splitting phenomenon on the surface of the growing EAFP crystal leads to a more complicated kinetic pattern of the step growth. Evidently, the advancement of steps in troop will bring multiple growth steps together to be developed as groups, in turn, to speed the rate of crystal growth. Besides, the additional growth sources produced by constantly splitting of steps are also favourable for the rapid growth of EAFP crystals. The observations show a mechanism governed by the advancement of trooped growth steps and the extra dislocation source owing to the splitting of steps, by which the fast growth of EAFP crystals could be attained.

The section analysis (see Fig. 4) revealed that the height of growth step on the {100} surface generated either by two dimensional nucleation at higher supersaturation or by screw dislocations at lower supersaturation were equal to the unit-cell parameter a (average of $\sim$2 nm), which is nearly perpendicular to the imaging surface of the crystal. In the case of this screw dislocation, the principal geometric characteristic of the dislocation, *i.e.* the Burger vector, is parallel to the dislocation and equal to the screw pitch, d_{100}, with a length of 2 nm. The shape of two-dimensional islands and dislocation spirals suggest that there is strong kinetic anisotropy in the step movement for growing crystals of EAFP.

3.2. Thermodynamic and kinetic parameters

Compared with other protein crystals, EAFP crystals are unusual in some aspects: (i) they contain a very low fraction of solvent ($V_M = 1.64$ Å^3 Da^{-1}, as seen below) and consequently show very tight packing of the protein molecules, (ii) the pH seems to have little

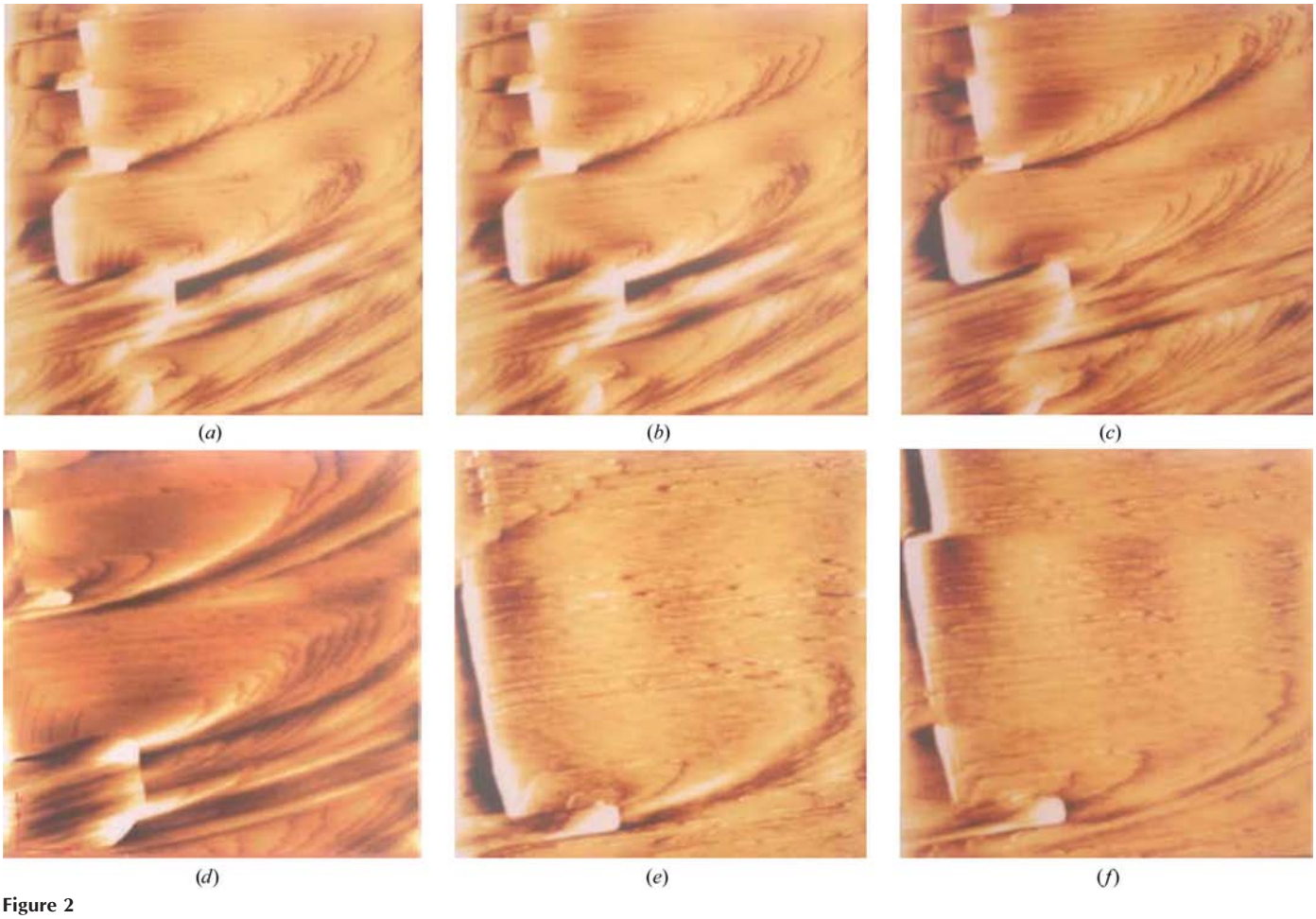

Figure 2
Sequential *in situ* AFM images collected at $\sim$5 min time intervals, showing the extensive appearance and development of multilayer stacks and active growth sources on the existing {100} surface of a growing EAFP crystal and their alternate generation and evolution controlled by the 2_1 axis along the crystallographic b axis. The complex multiple-layered stacks are responsible for its rapid growth at higher supersaturation. The first five images (15 × 15 µm) are taken at 0 (*a*), 5 (*b*), 10 (*c*) and 15 (*d*) min, respectively, showing two-dimensional nuclei and their stacks on the growing surface. (*e*) and (*f*) are images showing the surface features after incorporation of multi-stack two-dimensional nuclei into a growing EAFP crystal.

effect on the crystal growth, as the crystals could be obtained over a wide range of pH values, (iii) the high rigidity and stability of the molecular backbone structure which is cross-linked by five disulfide bridges and (iv) the crystals appear as flat long pieces which correspond to {100} faces within a few hours after crystallization set up. All these factors could make the thermodynamic and kinetic parameters of EAFP crystal growth unique.

The fundamental growth parameter, α, for the free energy of the step edge per unit step height and the kinetic coefficient, β, for step motion have been determined in several macromolecular crystallizations. All of the measurements show that these values in biological macromolecular crystallization are remarkably smaller than that in small molecular crystals (Land *et al.*, 1995; Malkin *et al.*, 1995, 1996, 1999; McPherson, 1999). This corresponds to most of the unique features in crystal growth of macromolecules. In the EAFP crystallization, the corresponding values estimated from AFM measurements are distinct from those for general protein crystallization. The value of α is approximately 68.6 erg cm^{-2} at the present supersaturation, which is much greater than that of other macromolecular crystals, but comparable with those of small-molecular crystals. The larger α value is most likely owing to the small solvent content in EAFP crystal. The measurement indicates that the thermodynamic properties such as tight packing and structural rigidity of EAFP crystal are similar to those of small molecules. On the other hand, the kinetic coefficient β is 6.9×10^{-4} cm s^{-1}, which is comparable to those determined from recent AFM studies of other macromolecular crystals. These data suggest that the EAFP molecule possesses a dual behaviour in crystallization: thermodynamically as a small molecule and kinetically as a macromolecule.

These fundamental thermodynamic and kinetic parameters governing EAFP crystal growth should be responsible for its unique behaviour in crystallization.

3.3. Molecular interactions and crystal packing

The analyses of molecular interactions and molecular packing in EAFP crystals were carried out by X-ray crystallography, which will provide some molecular basis for the AFM observations. The preliminary X-ray diffraction analysis showed that the crystal of EAFP belongs to the monoclinic form with space group $P2_1$, with unit-cell parameters $a = 19.01$, $b = 23.16$, $c = 30.69$ Å, $\beta = 98.54^\circ$. There is one EAFP molecule in the asymmetric unit, from which the value of the Matthews V_M is estimated to be 1.64 Å^3 Da^{-1} and the solvent content in the unit cell is 21%. Surveying most protein crystals, the values of V_M are generally in range between 1.68 and 3.53 Å^3 Da^{-1} (Matthews, 1968), which have been used in protein crystallography as a reference to solvent content. Evidently, the solvent content of EAFP crystals is lower to a minimum for the general protein crystals. Besides, the overall temperature factor (B value) calculated from the Wilson's statistics for EAFP structural model is 12 Å^2, which is also at the

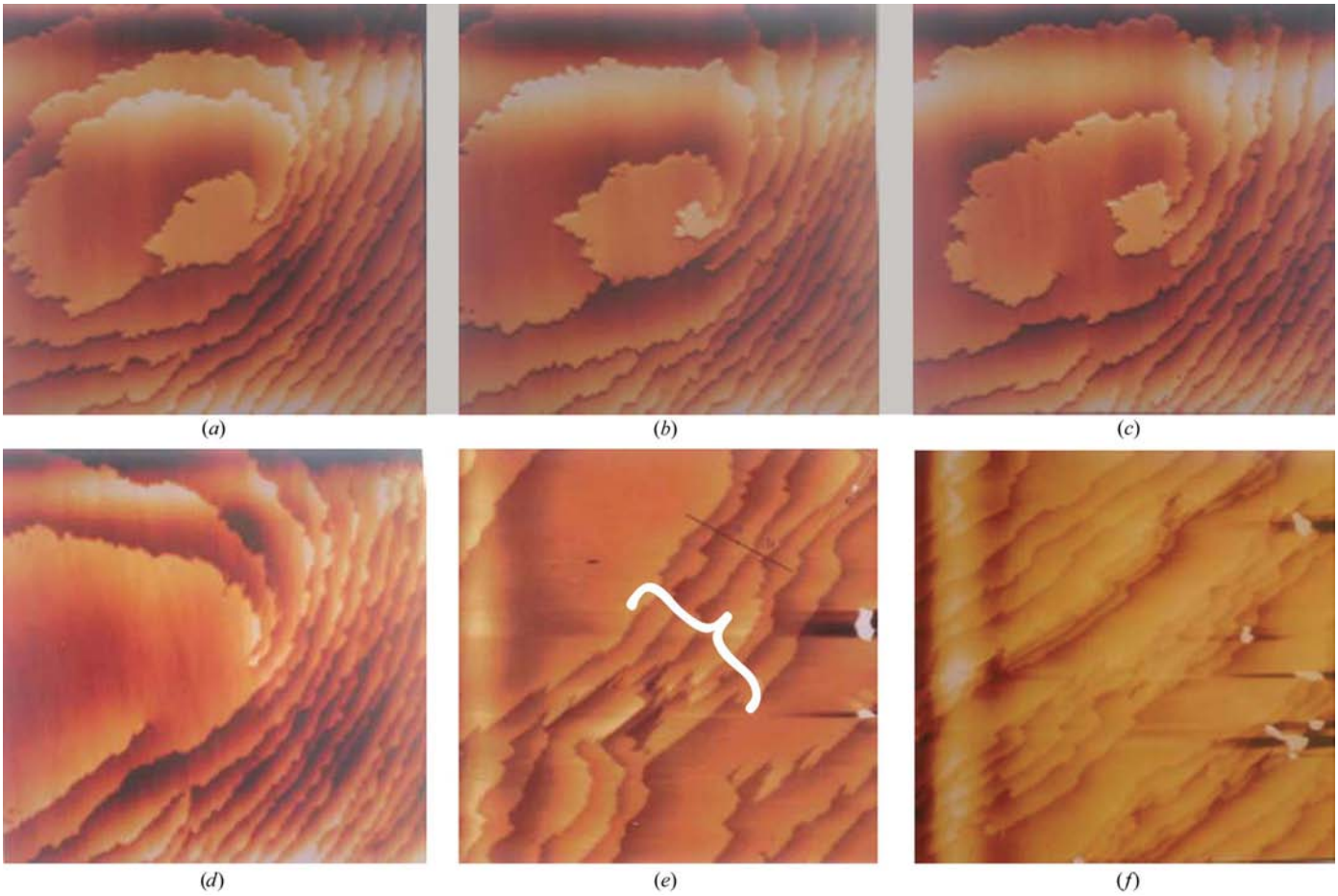

Figure 3
Images at low supersaturation condition showing the anisotropic single, double screw dislocation. The images show outcrops on the {100} surface of monoclinic EAFP crystal in (*a*), (*b*), (*c*) and (*d*), respectively. Scanning areas for images (*a*–*d*) are 15 × 15 µm. (*e*) and (*f*) show propagation of the troop of the multilayer steps which should be responsible for the rapid growth of crystals. The images are taken at $t = 0$ (*e*) and $t = 10$ min (*d*) and the scan areas are 10 × 10 µm and 20 × 20 µm for (*e*) and (*f*), respectively.

minimum for protein crystals. All these parameters are similar to those in small molecules and show extreme stability of EAFP crystals as indicated by the thermodynamic analysis described above.

The packing of EAFP molecules in the monoclinic crystal shows a unique scheme in which large monomolecular layers zigzag through the whole cell in the direction perpendicular to the crystallographic *a* axis (Fig. 5). Each EAFP molecule in the monoclinic $P2_1$ crystal lattice interacts with eight adjacent symmetry-related molecules (defined as $d < 4.0$ Å), while six molecules are associated tightly head to tail in zigzags along ⟨101⟩ in the crystallographic *bc* plane. In this way, an approximate hexagonal array of *ABABAB* along the [010] direction is formed within these layers. The molecules are related to each other by a translation of *b* and a rotation of 180°, so that there are twofold screw axis in the same molecular layer. The remaining two molecules with same orientation are above and below the plane in the opposite direction (by *a*) and are involved in weak molecular interactions, as shown in Fig. 5. With this organization, the molecular

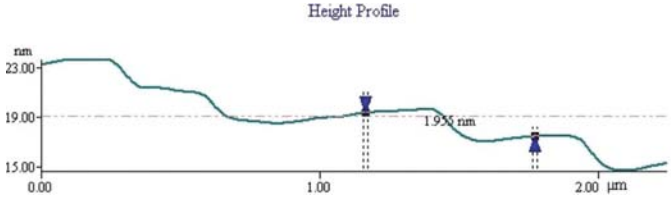

Figure 4
The section analysis indicating the height of a step in multilayer steps, *i.e.* the trooped steps at lower concentration. The corresponding troop of the multi-layer steps is indicated as a black line *ab* and a white single brace in Fig. 3(*f*).

Table 1
Molecular interactions in the monoclinic EAFP crystal.

Molecule at *x*, *y*, *z*					
Residue	Atom	Distance (Å)	Residue	Symmetry-related atom (including water-mediated)	Symmetry operation
Ser5	O	2.85	Asn34	ND2	[010] direction
Asn12	OD1	2.97	Ser25	N	
Asn12	ND2	2.70	Ser25	O	
Ser5	O	3.10	Water 24	O 2.73 Ala28 O	
Arg6	NE	3.2	Water 23	O 2.92 Arg9 O	
Arg6	NE	2.87	Water 44	O 3.20 Arg40 NE	
Cys7	O	2.54	Water 29	O 3.13 Alal27 O	
Pro8	O	2.57	Water 18	O 2.90 Gln38 N	
Arg9	O	2.92	Water 23	O 3.40 Pro10 O	
Pro10	O	2.93	Water 12	O 2.81 Ser25 OG	
No. of VDW contacts: 28					
Asn12	OD1	2.44	Arg40	NH2	⟨110⟩ direction
Arg40	O	2.95	Ala27	N	
Arg9	O	2.89	Water 7	O 3.01 Ala27 N	
Arg9	NH2	2.68	Water 3	O 2.76 Gly14 O	
No. of VDW contacts: 46					
Alal27	N	2.95	Arg40	O	⟨101⟩ direction
Gly33	O	3.17	Arg36	NE	
Ala32	O	2.93	Water 40	O 2.69 Ile19 O	
No. of VDW contacts: 22					
Ser25	N	2.97	Asn12	OD1	⟨011⟩ direction
Ser25	O	2.70	Asn12	ND2	
Tyr22	OH	2.81	Arg36	O	[100] direction
Ala27	N	2.95	Arg40	O	
Arg9	NE	3.01	Water 14	O 2.81 Cys39 N	
Cys23	O	3.05	Water 28	O 2.86 Arg40 NH2	
No. of VDW contacts: 69					

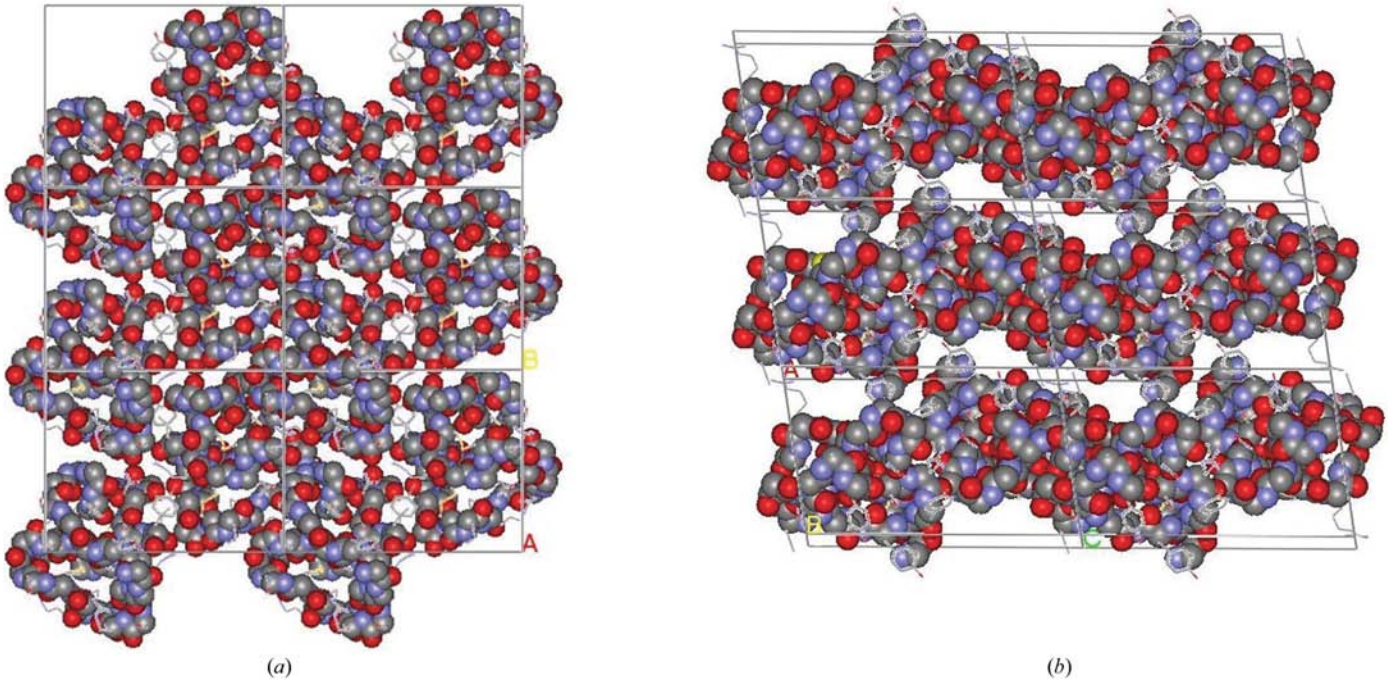

Figure 5
Molecular packing in the monoclinic EAFP crystal as viewed along the crystallographic *a* axis (the upper left) and the *b* axis (the upper right and the below). The molecular backbone was represented with CPK and the surface side chains exposed to solvent area with steak. For the clarity, the solvent molecules are not shown. One molecule was assigned a position based on the AFM image or X-ray crystallography results and the remaining molecules in the unit cell were generated by space-group operations. It is clear that the zigzag molecular layer is perpendicular to *a* axis approximately. The molecules in these pseudo-hexagonal layers are stacked in *ABABAB* along [010] direction. Each layer is related to the one above or below by 180° rotation (the 2_1 screw) parallel to the layer. The solvent channels run parallel to the {100} layers. The intermolecular contacts between EAFP molecules are listed in Table 1.

layers are parallel to the *bc* plane and nearly perpendicular to [100] direction at an interval of *a*. This packing mode gives rise to very tight assembly of EAFP molecule and high orderliness of crystals, which are coincident with the properties of EAFP crystal growth from AFM observation.

The intermolecular interactions in such packing were analyzed using the program *CONTACT* (*CCP*4 suite; Collaborative Computational Project, Number 4, 1994) and the result is listed in Table 1. The dominant contacts appears at the molecular interface along ⟨101⟩, ⟨011⟩, [010] and [001] directions, including 13 hydrogen bonds between main-chain NH and CO groups (see Table 1). The molecular layers perpendicular to the [100] direction showed a few hydrogen bonds including rather weak interactions between molecules in crystallographic *a* axis. It seems that the hydrogen bonds between the rigid peptide backbones of the neighbouring (*e.g.* adjacent molecules along ⟨110⟩ direction) on the monomolecular layer contribute more to stability of the crystal lattice. In addition, there are numerous van der Waals contacts in between the molecular surfaces in all direction of the unit cell. Obviously, the tight crystal packing of EAFP molecules is mainly dominated by a large number of non-bonded interactions as in general protein crystals, but for the EAFP crystal it features more direct hydrogen bonds between EAFP molecules.

In addition, the elementary growth layers and the growth behaviour of EAFP crystals described above correspond well to the periodic bond chains (PBC) theory (Hartman & Perdok, 1955*a*,*b*,*c*; Hartman, 1973; Frey *et al.*, 1991; Chernov, 1998) on the basis of the distribution and strength of bonds within EAFP crystal structure. The strength of each contact between molecules in the unit cell was estimated by counting the number of direct hydrogen bonds between residue atoms, water-mediated atoms and assumed van der Waals interactions involved in the contacts, owing to the lack of thermodynamic and bonding-energy parameters of this new protein EAFP.

According to the Hartman's theory (Hartman & Perdok, 1955*a*,*b*,*c*), the most developed {100} face is the growth slice (the minimum thickness of the growth layer) containing three uninterrupted chains of strong bonds along ⟨011⟩, [010] and [001] direction within thickness d_{100} and consequently the repeat period of the surface (100) has to be $d_{100} \simeq 2$ nm, which indicates that a repeatable growth step is just the size of one EAFP molecule.

4. Concluding remarks

The growth kinetics of EAFP monoclinic crystal with a fast growth rate has been investigated by observing *in situ* AFM images at defined supersaturation. Although the EAFP crystallization basically follows the general growth mechanisms observed in other biomacromolecular crystallization, there are several remarkable features which may be responsible for the unusually rapid growth of EAFP crystals, including (i) fast occurrence of the growth sources with strong asymmetric multi two-dimensional island stacking, (ii) the variety of types of strong anisotropic spiral dislocation growth sources (the double left-handed spiral source as a main source and the single right-handed as a minor source), (iii) constant generation of the step splitting (one divides into two) during the process of growth or generation of new steps at or near the centre of main growth spiral and (iv) growth by extension of the trooped steps, with which extension of growth steps also in troop. The propagation of the steps through strapping growth steps together should be faster than single advancement in turn to speed up the rate of growth. The height of each growth step on the {100} surface was equal to one unit-cell parameter *a* (average of 2 nm). Moreover, the occurrence and development of the active growth sources on the {100} surfaces are controlled and related by the 2_1 screw rotation axis along the crystallographic *b* axis. All features show a possible mechanism by which the unusual fast growth of EAFP crystals could be attained.

This work was supported by Chinese Academy of Sciences grant (Nos. KSCX2-SW-322, KSCX2-SW-17) and the MOST of China (2002BA711A13). The X-ray characterization work was supported by the Photon Factory of KEK, Japan (2002G310). We are indebted to Professor W. R. Hu for his continuous encouragement of this work.

References

Astier, J. P., Bokern, D., Lapena, L. & Veesler, S. (2001). *J. Cryst. Growth*, **226**, 294–302.
Chernov, A. A. (1998). *Acta Cryst.* A**54**, 859–872.
Collaborative Computational Project, Number 4 (1994). *Acta Cryst.* D**50**, 760–763.
Durbin, S. D. & Carlson, W. E. (1992). *J. Cryst. Growth*, **122**, 71–79.
Frey, M., Genoveio-Taverne, J.-C. & Fontecilla-Camps, J. (1991). *J. Phys. D*, **24**, 105–110.
Hartman, P. (1973). Editor. *Crystal Growth, An Introduction*, pp. 367–402. Amsterdam: North Holland.
Hartman, P. & Perdok, W. G. (1955*a*). *Acta Cryst.* **8**, 49–52.
Hartman, P. & Perdok, W. G. (1955*b*). *Acta Cryst.* **8**, 521–524.
Hartman, P. & Perdok, W. G. (1955*c*). *Acta Cryst.* **8**, 525–529.
Huang, R. H., Xiang, Y., Liu, X. Z., Zhang, Y., Hu, Z. & Wang, D.-C. (2002). *FEBS Lett.* **521**, 87–90.
Jones, T. A., Zou, J. Y., Cowan, S. W. & Kjeldgaard, M. (1991). *Acta Cryst.* A**47**, 110–119.
Kuznetsov, Yu. G., Land, T. A., DeYoreo, J. J. & McPherson, A. (1995). *Nature Struct. Biol.* **2**, 956–959.
Kuznetsov, Yu. G., Malkin, A. J., Glantz, W. & McPherson, A. (1996). *J. Cryst. Growth*, **168**, 63–73.
Land, T. A. & De Yoreo, J. J. (2000). *J. Cryst. Growth*, **208**, 623–637.
Land, T. A., Malkin, A. J., Kuznetsov, Yu. G., McPherson, A. & DeYoreo, J. J. (1995). *Phys. Rev. Lett.* **75**, 2774–2777.
Liu, X.-Z., Hu, Z., Li, Y., Yang, J.-B. & Li, B.-J. (1994). *Acta Bot. Yunnan.* **16**, 385–391.
McPherson, A. (1999). *Crystallization of Biological Macromolecules*, p. 395. New York: Cold Spring Harbor Laboratory Press.
McPherson, A., Malkin A. J., Kuznetsov, Yu. G. & Koszelak, S. (1996). *J. Cryst. Growth*, **168**, 74–92.
McPherson, A., Malkin, A. J., Kuznetsov, Yu. G. & Plomp, M. (2001). *Acta Cryst.* D**57**, 1053–1060.
Malkin, A. J., Kuznetsov, Yu. G. & McPherson, A. (1996). *J. Struct. Biol.* **117**, 124–137.
Malkin, A. J., Kuznetsov, Yu. G. & McPherson, A. (1999). *J. Cryst. Growth*, **196**, 471–488.
Malkin, A. J., Land, T. A., Kuznetsov, Yu. G., McPherson, A. & De Yoreo, J. J. (1995). *Phys. Rev. Lett.* **75**, 2778–2781.
Matthews, B. W. (1968). *J. Mol. Biol.* **33**, 491–497.
Xiang, Y., Huang, R.-H., Liu, W., Li, G., Liu, X.-Z. & Wang, D.-C. (2002). *Acta Cryst.* D**58**, 1838–1840.
Xiang, Y., Huang, R.-H., Liu, X.-Z., Zhang, Y. & Wang, D.-C. (2004). *J. Struct. Biol.* **148**, 86–97.
Yip, C. M. & Ward, M. D. (1996). *Biophys. J.* **71**, 1071–1078.